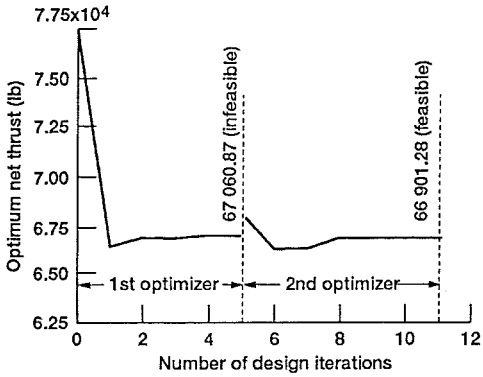

Fig. 3 Cascade solution for a wave–rotor-topped subsonic engine.

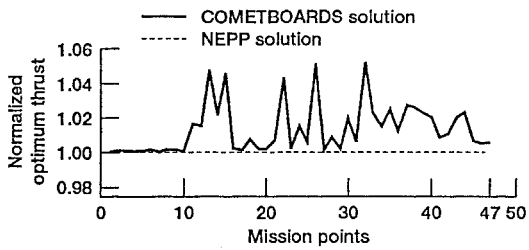

Fig. 4 Value-added benefit in design of a 47-mission-point, high-bypass-turbofan subsonic engine using a wave rotor.

ciated with the wave rotor were active. The active variables considered were the rotational speed of the wave rotor and the heat added to the wave rotor. Important active constraints included the limits on maximum speeds of the compressors, a 15% surge margin for all compressors, and a maximum wave–rotor exit temperature. The engine thrust was selected as the merit function. The wave–rotor–engine design became a sequence of 47 optimization subproblems, one for each mission point. Only by using the cascade strategy could the problem be solved successfully for the entire flight envelop. For the mission point defined by Mach number = 0.1 and altitude = 5000 ft, the convergence of the two-optimizer cascade strategy is shown in Fig. 3. The first optimizer produced an infeasible design at 67,060.87-lb thrust in about five design iterations. The second optimizer, starting from the first solution with a small perturbation, produced a feasible optimum design with an optimum thrust of 66,901.28 lb. The optimum solutions for the 47 mission points obtained by using the combined tool were normalized with respect to the NEPP results and are shown in Fig. 4. The combined tool produced a higher thrust than the NEPP for mission points 12, 26, and 32. Both NEPP and COMETBOARDS–NEPP produced identical optimum thrust values for a few mission points. The maximum difference in thrust exceeded 5% for several mission points. These differences could be significant if the design points with increased thrust were used to size the engine. The combined COMETBOARDS–NEPP tool successfully solved the subsonic wave–rotor–engine design optimization problem.

Conclusions

Combined code COMETBOARDS with FLOPS and NEPP successfully solved a number of aircraft and engine design problems. The advanced features and unique strengths of COMETBOARDS made subsonic and supersonic aircraft design problems and engine-cycle design problems easier to solve. The cascade optimization strategy was especially helpful in generating feasible optimum solutions when an individual optimizer encountered difficulty. The cascade strategy converged to the same optimum design, even when it started from different initial design points. The research-level software COMETBOARDS, with some enhancement and modification, can be used by the aircraft industry to design aircraft and their engines.

References

[1]McCullers, L. A., and Sobieski, J. (eds.), "FLOPS: Aircraft Configuration Optimization Including Optimized Flight Profiles," NASA CP-2327, April 1984.

[2]Klann, J. N., and Snyder, C. A., "NEPP Programmers Manual," NASA TM-106575, Sept. 1994.

[3]Guptill, J. D., Coroneos, R. M., Patnaik, S. N., Hopkins, D. A., and Berke, L., "COMETBOARDS Users Manual," NASA TM-4537, 1996.

[4]RPK_NASTRAN, COSMIC, University of Georgia, Athens, GA, 1994.

[5]Patnaik, S. N., Coroneos, R. M., Guptill, J. D., and Hopkins, D. A., "Comparative Evaluation of Different Optimization Algorithms for Structural Design Applications," *International Journal for Numerical Methods in Engineering*, Vol. 39, No. 10, 1996, pp. 1761–1774.

[6]Patnaik, S. N., Gendy, A. S., and Hopkins, D. A., "Design Optimization of Large Structural Systems with Substructuring in a Parallel Computational Environment," *Computing Systems in Engineering*, Vol. 5, Nos. 4–6, 1994, pp. 425–440.

Aerodynamic Characteristics of the F/A-18 at Large Roll Angles and High Incidence

B. H. K. Lee* and D. Brown†
National Research Council,
Ottawa, Ontario K1A 0R6, Canada

Introduction

WIND-TUNNEL measurements on various models of the F/A-18 aircraft have been conducted in several laboratories in the U.S. The scales of the models range from full size at NASA Ames Research Center[1] to 16% at NASA Langley Research Center,[2] and 6% at David Taylor Research Center.[3] By and large, the wind-tunnel programs have been devoted to force, moment, and pressure distribution measurements, in symmetrical flow conditions, at angles of attack up to 50 deg with some emphasis on flow visualization.

In Canada, a wind-tunnel program was initiated in 1988 to investigate tail buffet on the F/A-18 using a 6% scale model. Tests were performed with the model oscillating in pitch and roll to study the hysteresis effect of vortex burst on tail buffet.[4] In those experiments, stability derivatives were measured, but the oscillation frequencies were very low because of limitations of the Institute for Aerospace Research (IAR) sting support system, thus making the results of limited use. However, static lateral stability characteristics were also investigated. This Note presents some results on roll stability that complement the weathercock stability data given by Erickson et al.[3]

Model

The model used is a rigid 6% scale model of the F/A-18. It consists of three major pieces: 1) an aluminum forebody with integral leading-edge extension (LEX) and a single seat can-

Received Oct. 1, 1996; revision received Oct. 24, 1996; accepted for publication Oct. 25, 1996. Copyright © 1996 by B. H. K. Lee and D. Brown. Published by the American Institute of Aeronautics and Astronautics, Inc., with permission.

*Group Leader, Institute for Aerospace Research. Experimental Aerodynamics and Aeroelasticity. Associate Fellow AIAA.

†Institute for Aerospace Research (Retired). Member AIAA.

opy, 2) a stainless-steel fuselage with integral wings, and 3) a stainless-steel rear fuselage. The center fuselage was bored to accept a 3.81-cm-diam six-component sting balance. Scaled AIM-9 missiles were mounted on the wing tips. For these measurements, the leading- and trailing-edge flaps were set at 34 and 0 deg, respectively, and the horizontal stabilator angle was set at −9 deg. These angles correspond to the F/A-18 auto flaps-up mode schedule settings at high angles of attack. Boundary-layer transition trips were installed on the wings, LEX, fins, stabilators, and forebody of the model. A more detailed description of the model is given in Ref. 5.

The test model was mounted in the IAR 1.5 × 1.5 m trisonic blowdown wind tunnel on a cranked sting that forms part of the model support system. The strut can be programmed to move vertically and through the pitch linkage mechanism, the model angle of attack can vary from 0 to 33 deg. For high Mach numbers and dynamic pressures, aerodynamic loading causes bending of the sting that can increase the angle of attack by up to 2 deg. The tests were carried out at several subsonic Mach numbers, angles of attack, and roll angles between ±30 deg, but only results at $M = 0.6$ and 0.8 and $\alpha = 20$ and 30 deg are presented in this Note. The Reynolds numbers based on the model mean aerodynamic chord are 3.38×10^6 and 4×10^6, respectively.

Static Roll Characteristics

The coordinate system and the sign convention for definition of the forces and moments follow the standard notations used in the literature. The subscript b denotes coefficients based on body axes. The wing mean aerodynamic chord and reference wing area used to compute the cofficients are 0.21 m and 0.134 m^2, respectively.

Figure 1 shows the variations in lift coefficient C_L with roll angle for $\alpha = 20$ and 30 deg at $M = 0.6$ and 0.8. At the lower α, C_L is slightly larger at $M = 0.6$ than at 0.8 over the whole roll range, whereas at $\alpha = 30$ deg, the reverse holds for $-15 < \phi < 20$ deg. Outside this range, larger C_L are exhibited at $M = 0.6$. The curves have a small asymmetry about the roll angle $\phi = 0$ deg, with C_L slightly higher for negative ϕ. It is not certain where this asymmetry arises, although model imperfection can be ruled out. A possible explanation is the varying spatial flow quality of the wind tunnel. At high incidence, the roll of the model on the cranked sting places a significant part of the model in a different region of the flowfield in the wind tunnel. (The c.g. of the model remains fixed relative to the tunnel, and a 11-deg offset in the cranked sting produces a fair-size cone angle, considering the model length is 99.56 cm with the c.g. 62.73 cm from the nose.) Some flow quality measurements in the wind tunnel are required to confirm this possible explanation.

The shape of the drag coefficient curves at $\alpha = 20$ and 30 deg is shown in Fig. 2. Larger drag values are observed at the higher M and they are consistently greater than those at $M = 0.6$. The asymmetry of the curves for positive and negative ϕ is less than those found in C_L.

Figure 3 illustrates the dependence of rolling-moment coefficient C_{lb} on ϕ. At $\alpha = 20$ deg, adequate static roll stability, as defined by a negative $\partial C_{lb}/\partial\phi$, exists at $M = 0.6$ and 0.8 over the range of ϕ investigated. However, at $\alpha = 30$ deg, while stabilty is maintained at $M = 0.6$ in the range -30 deg $< \phi < 30$ deg, this is not true at $M = 0.8$, where $\partial C_{lb}/\partial\phi$ is

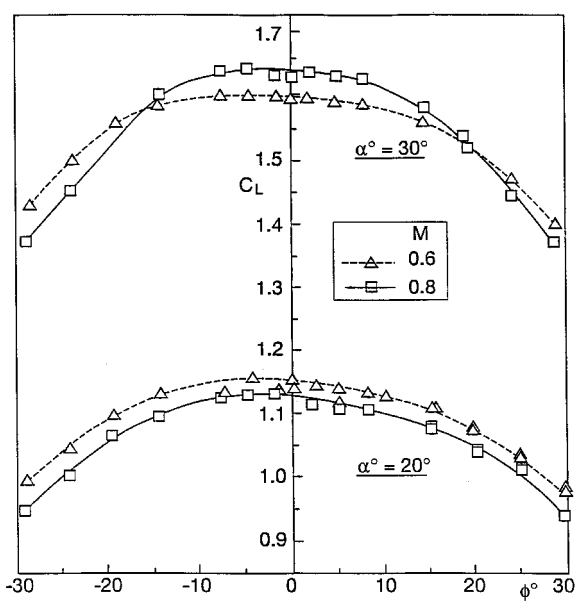

Fig. 1 Lift coefficient vs roll angle.

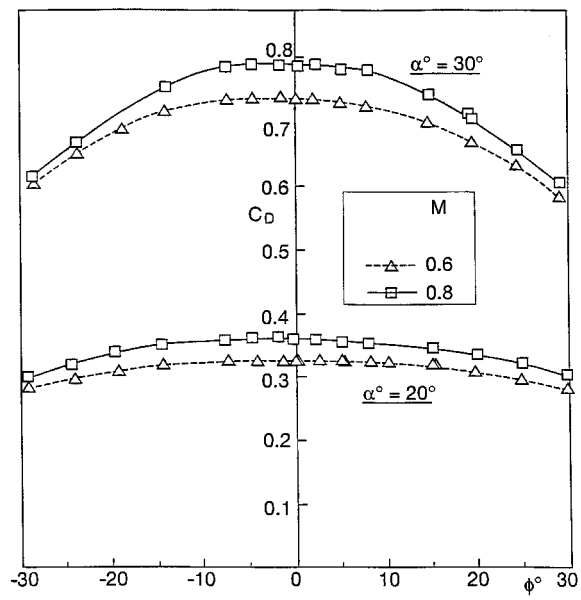

Fig. 2 Drag coefficient vs roll angle.

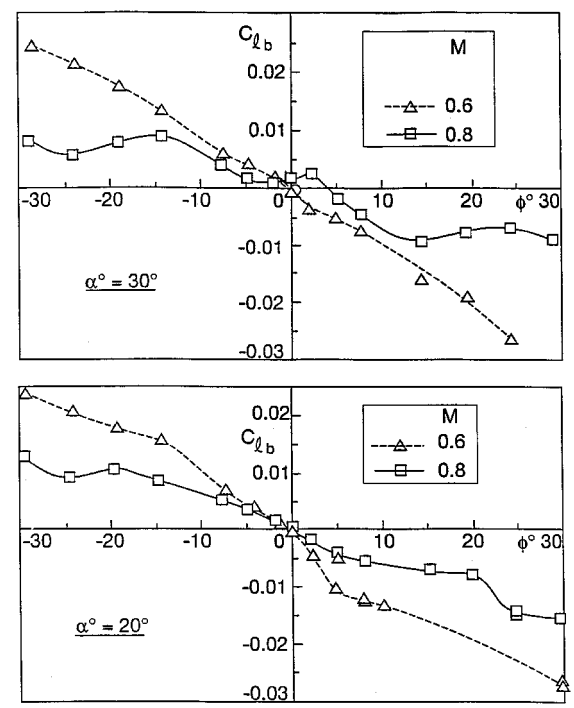

Fig. 3 Rolling-moment coefficient vs roll angle.

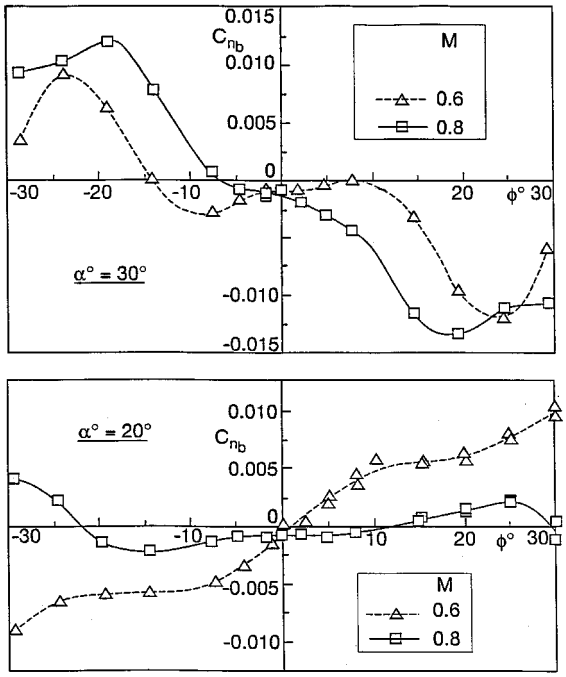

Fig. 4 Yawing-moment coefficient vs roll angle.

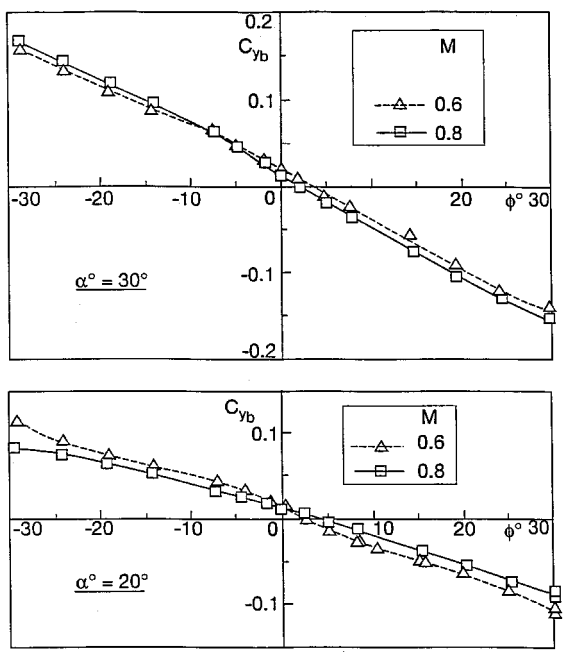

Fig. 5 Side-force coefficient vs roll angle.

nearly zero or slightly positive for $|\phi| > 14$ deg. The exact slope cannot be determined with accuracy because of the experimental uncertainties. Between $-14 < \phi < 14$ deg, $\partial C_{lb}/\partial\phi$ is negative and its value is small when the points at $\phi = 0$ and 2.5 deg are ignored.

As is well known, roll–yaw motions are inextricably coupled and meaningful conclusions on lateral behavior of the aircraft can only be derived from dynamic analysis. However, the static derivatives are still useful to give some information of the aircraft characteristics. The yawing moment C_{nb} is shown in Fig. 4. At $\alpha = 20$ deg, $\partial C_{nb}/\partial\phi$ is positive over the entire roll range for $M = 0.6$, whereas at $M = 0.8$, $\partial C_{nb}/\partial\phi$ is approximately zero for $-20 < \phi < 10$ deg. At $\alpha = 30$ deg, the curves are quite different from those at 20 deg. Large negative slopes are observed outside the range $-7.5 < \phi < 7.5$ deg. They become zero at about ± 25 deg for $M = 0.6$ and ± 17.5 deg for $M = 0.8$. Thereafter, the slope becomes positive. There are significant variations of $\partial C_{nb}/\partial\phi$ with ϕ at high α. A slight offset of the curves at $\phi = 0$ deg is observed and this is more noticeable at the higher α. An explanation for this behavior is similar to that previously given for the C_L curves. Figure 5 shows the relation between the side-force coefficient C_{yb} and ϕ. $\partial C_{yb}/\partial\phi$ is negative over the entire range of ϕ investigated and a reasonably constant slope for C_{yb} with ϕ is observed. Once more, a small offset of the curves is detected at the origin that is attributed to flow nonuniformity in the wind tunnel.

In summary, both C_L and C_D exhibit a decrease with ϕ. $\partial C_{yb}/\partial\phi$ is practically constant over the whole excursion in ϕ, and the effect of M is small. Good roll stabilty is maintained up to $\phi = 30$ deg for $M = 0.6$, whereas at $M = 0.8$, stability deteriorates and becomes marginally stable at values of ϕ larger than 14 deg. M and α effects are quite pronounced for C_{nb}.

References

[1]Meyn, L. A., Lanser, W. R., and Kevin, D. J., "Full Scale High Angle of Attack Tests of an F/A-18," AIAA Paper 92-2676, June 1992.

[2]Banks, W. D., "Wind Tunnel Investigation of the Forebody Aerodynamics of a Vortex-Lift Fighter Configuration at High Angles of Attack," Society of Automotive Engineers, Paper 881419, Oct. 1988.

[3]Erickson, G. E., Hall, R. M., Banks, D. W., Del Frate, J. H., Schriener, J. A., Hanley, R. J., and Pulley, C. T., "Experimental Investigation of the F/A-18 Vortex Flows at Subsonic Through Transonic Speeds, Invited Paper," AIAA Paper 89-2222, July 1989.

[4]Lee, B. H. K., and Tang, F. C., "Unsteady Pressure and Load Measurements on an F/A-18 Vertical Fin," *Journal of Aircraft*, Vol. 30, No. 5, 1993, pp. 756–762.

[5]Lee, B. H. K., and Brown, D., "Wind-Tunnel Studies of F/A-18 Tail Buffet," *Journal of Aircraft*, Vol. 29, No. 1, 1992, pp. 146–152.

Aircraft Engine Bay Cooling and Ventilation: Design and Modeling

Corin Segal*
University of Florida, Gainesville, Florida 32611

Introduction

THE modern generation of military airplanes are equipped with low-bypass turbofans with relatively cool engine casings. In some instances the bypass ratio is very low [0.2–0.4 (Ref. 1)] and these engines are often called cooled turbojets. Because of the low temperatures at the engine surface engine, bay cooling is not, in general, as stringent a requirement as the ventilation of the bay of potentially flammable gas mixtures resulting from leaks between various modules of the engine. In flight, unidirectional ventilation air is, in general, relatively easy to achieve by a careful design of inlet scoops and outlets that take advantage of the air ram and the existence of low-pressure regions on the rear part of the airplane fuselage. The difficulty is to obtain sufficient ventilation on the ground, at static conditions.

Figure 1 shows a number of engine bay ventilation schemes implemented on some of the airplanes currently in service. Figure 1a shows the scheme adopted for the F-15. Engine bay

Received Aug. 31, 1995; revision received April 7, 1996; accepted for publication Nov. 1, 1996. Copyright © 1996 by C. Segal. Published by the American Institute of Aeronautics and Astronautics, Inc., with permission.

*Assistant Professor, Aerospace Engineering, Mechanics and Engineering Science. Senior Member AIAA.